Journal of Membrane Science 361 (2010) 213–222

Contents lists available at ScienceDirect

Journal of Membrane Science

journal homepage: www.elsevier.com/locate/memsci

Effect of the metal oxide particle distributions on modified PES membranes characteristics and performance

Nermen Maximous, G. Nakhla*, W. Wan, K. Wong

Department of Chemical and Biochemical Engineering, Faculty of Engineering, University of Western Ontario, 1151 Richmond Street, London, Ont., Canada N6A 5B9

ARTICLE INFO

Article history:
Received 12 April 2010
Received in revised form 19 May 2010
Accepted 23 May 2010
Available online 31 May 2010

Keywords:
Al_2O_3
ZrO_2
Membrane bioreactor
Fouling mitigation
Activated sludge

ABSTRACT

In this study, the effect of metal oxide particle distribution pattern on the performance and physical characteristics of 0.03, 0.05 and 0.1 Al_2O_3/PES and ZrO_2/PES composite membranes was investigated. Membrane morphology was characterized by field-emission scanning electron microscopy (FESEM) and the metal oxides particles distribution patterns were determined using Image J software (U.S. National Institutes of Health, Bethesda, MD, USA). The prepared metal oxides/PES membranes were skin-type membranes and showed a structural change from finger- to sponge-type structure. The finger structure was associated with high metal oxides percentage of the total metal oxide particles entrapped in the membrane (60–95% and 52–100% for Al_2O_3/PES and ZrO_2/PES, respectively) in the membrane matrix. No statistical correlations have been observed between either the particles densities at the 0–10 or 10–20 μm depths and membrane physical characteristics or performance parameters. However, strong inverse correlations were observed between the metal oxides particles densities at the membranes depths of 30–40 and 40–50 μm, respectively, and membrane fouling resistances (R_f). According to the constant pressure models, the experimental results for sludge filtration using all tested membranes were in good agreement with the standard blocking model (SBM).

1. Introduction

The effect of membrane morphology and surface chemistry on fouling mechanisms has been studied by many researchers with various biological fluids, particularly protein solutions. Extensive works [1–4] attributed lower fouling to smooth hydrophilic membranes with high porosity and narrow pore size distribution. Metsamuuronen et al. [5] reported that much lower critical fluxes were observed for the ultrafiltration of baker's yeast when a hydrophobic polysulfone membrane was used as opposed to a hydrophilic regenerated cellulose membrane.

Surface modification of membranes is an attractive approach to change the surface properties of the membrane in a defined selective way while preserving its macroporous structure. Recently, considerable effort has been devoted to the fabrication of metal oxides/polymer composite membranes in order to develop photocatalytic membrane reactors [6–8] or to import anti-fouling properties to neat polymeric membranes [9–14].

Membrane roughness and porosity were suggested as potential reasons for the different fouling behaviors [15]. He et al. [16] reported that for the treatment of a high-strength food processing wastewater using an MBR, membranes with a larger molecular weight cut-off size fouled more rapidly and to a greater extent than the one with smaller molecular weight cut-off. These results suggested that membranes with a larger nominal pore size may foul more readily as a result of blocking by macro colloids, which can completely block the entrance of the pores. It is quite clear from the literature [17–21] that the pore size alone cannot predict hydraulic performances as no general trend was observed between these two parameters. The complex and changing nature of the biological suspension present in MBR systems and the large pore size distribution of the membrane generally used in MBR are the main reasons for the undefined general dependency of the flux propensity on pore size [17,21].

In our previous work [12–14], investigation of the effect of ZrO_2 or Al_2O_3 particles on the membrane fouling characteristic was studied by casting different weight ratios membranes of metal oxides/polyethersulfon (PES). The results showed that metal oxides entrapped membranes showed lower flux decline during activated sludge filtration compared to neat polymeric membranes. However, previous studies of blending membranes with metal oxides particles focused primarily on membrane performance and over looked the effect of the metal oxides particles distribution pattern on the membrane performance and structure [6–14]. Although literature studies did not address the impact of membrane preparation conditions on metal oxide distributions, it is expected that the solvent evaporation time, polymer concentrations, and com-

* Corresponding author. Tel.: +1 519 661 2111.
E-mail addresses: nmaximou@uwo.ca (N. Maximous), gnakhla@eng.uwo.ca (G. Nakhla), wkwan@eng.uwo.ca (W. Wan), khwong@uwo.ca (K. Wong).

0376-7388/$ – see front matter © 2010 Elsevier B.V. All rights reserved.
doi:10.1016/j.memsci.2010.05.051

positions of the precipitant will impact the particles distribution patterns, with the role of the aforementioned process variables requiring further investigation. Therefore, this research aims at investigating the effect of metal oxide particles distribution pattern on the performance and physical characteristics of Al_2O_3/PES and ZrO_2/PES composite membranes. To eliminate the factor of particles load in the membrane casting solutions, membranes with same metal oxide/PES (w/w) ratios of 0.03, 0.05 and 0.1 were compared. The membranes morphology was characterized by field-emission scanning electron microscopy (FESEM) and the metal oxides particles distribution patterns were determined using Image J software (U.S. National Institutes of Health, Bethesda, MD, USA). The membranes strengths, molecular weight cut-off (MWCO), DIW permeability, filtration resistances and fouling rates were determined and compared.

2. Experimental

2.1. Membrane preparation

PES Radel A-100 (Solvay Advanced Polymers, Alpharetta, GA, USA) was used as a membrane material and metal oxide entrapped membranes of 0.03, 0.05 and 0.1 metal oxide/PES ratios (w/w) were prepared by phase inversion [22]. The detailed preparation method is presented in our previous work [12–14]

2.2. Membrane characterization and performance

The deionized water (DIW) flux was determined for the PES control membranes as well as the metal oxide/PES membranes at different TMPs of 0.345, 0.69, 1.034, 1.38 and 1.724 bars. The cross-sectional morphologies of the membranes were characterized using field-emission scanning electron microscopy (FESEM, Leo 1530, LEO Electron Microscopy Ltd) at 1 kV with no conductive coating. To expose the membrane cross-section for SEM characterization, the membranes were cryogenically fractured in liquid nitrogen. The distribution of the metal oxides particles, the dimensions of the membranes and the metal oxides particles density per membrane unit area were measured using the Java-based image processing program, Image J (U.S. National Institutes of Health, Bethesda, MD, USA). The effect of metal oxides particles on the membrane strength has been studied in terms of maximum TMP sustained by the tested membranes.

Molecular weight cut-off of the membranes was determined using 10% polyethylene oxide (PEO) MW 100, 200, 300 and 600 kDa aqueous solutions. The concentrations of PEO were measured using LEICA Auto ABBE refractometer model 100500B (Letica Co., Rochester, MI, USA) [23]. Rejection was calculated by Eq. (1):

$$\%R = \left(1 - \frac{C_{per}}{C_{feed}}\right) \times 100 \quad (1)$$

where C_{per} is the concentration of PEO in permeate and C_{feed} is the concentration of PEO in the feed. The smallest molecular weight that is rejected by 90% was taken as the MWCO of the membrane [23]. The membrane pores sizes were calculated using Eqs. (2) and (3) [24–27]

$$\text{Log } Rg = \nu \,\text{Log Mw} \quad (2)$$

where Mw is the polymer molecular weight in Da; Rg is the radius of gyration of the polymer in Å; ν is the linear fit coefficient (equal to 0.515 [25] or 0.583 [26])

$$Rh = 0.665\, Rg \quad (3)$$

where: Rh is the effective hydrodynamic radius of the polymer in solution.

The MWCO is an established method to measure the pore size as the comparison with crystal structures and electron micrographs indicated that the membrane pore radius, Rp, is close to the effective hydrodynamic radius of the polymer in solution, Rh, of the largest PEO able to diffuse through the pore or to block ion conductance [25].

The performances of the membranes were assessed based on the membranes resistances and pseudo steady-state fouling rates values during sludge filtration. Activated sludge used in this study was cultivated in a submerged laboratory scale MBR treating synthetic wastewater for more than 12 months. The sludge compositions and characteristics are mentioned elsewhere [12–14]. In order to alleviate the impact of compaction of the new polymeric membranes on flux, pre-filtration studies with pure deionized water (DIW) were conducted until a steady-state flux (J_{iw}) was achieved. During sludge filtration, the TMP and stirring speed were kept constant at 0.69 bar (as this is a typical TMP for submerged membranes like GE membranes, GE Oakville, ON) and 600 rpm, respectively. The permeate flux was determined by monitoring the volume of permeate with time. After the filtration test, the membrane was washed in a cross-flow manner with DIW, the pure DIW flux (J_{fw}) was measured four times after this cleaning regime. The degree of membrane fouling was calculated quantitatively using the resistance-in-series model [22].

$$J = \frac{\text{TMP}}{\eta R_t} \quad (4)$$

where J is the flux (L/m^2 h); TMP is the trans membrane pressure (0.69 bar); η is the viscosity of water at room temperature.

$$R_t = R_m + R_f + R_c \quad (5)$$

Resistances values were obtained by the following equations:

$$R_m = \frac{\text{TMP}}{\eta J_{iw}} \quad (6)$$

$$R_f = \frac{\text{TMP}}{(\eta J_{fw}) - R_m} \quad (7)$$

$$R_c = \frac{\text{TMP}}{(\eta J) - (R_m + R_f)} \quad (8)$$

where R_m is the intrinsic membrane resistance; R_f is the sum of the resistances caused by solute adsorption into the membrane pores or walls and chemically reversible cake; R_c is the cake resistance formed by cake layer deposited over the membrane surface.

Membrane fouling rate was calculated by fitting the experimental data using Sigma Plot software version 10 (Systat Software, Inc., Canada). The theoretical curves were generated by aforementioned software; the data fit the exponential decay (3-parameters) equation (Eq. (9)) with R^2 of 0.90–0.99.

$$y = y^{\circ} + ae^{-bt} \quad (9)$$

where y is the permeability (L/m^2 h-bar), t is the time (h), y° is the permeability at (t) equal infinity and a, b are the regression constants. The fouling rate was determined using Eq. (10).

$$\frac{dy}{dt} = -abe^{-bt} \quad (10)$$

The final fouling rates are the averages of dy/dt at five points at times varying between 2.5 and 3 h.

The fouling mechanism was investigated using Hermia's [28] constant pressure filtration models. The models assumed that the membranes have single pore sizes and the main forms of membrane fouling by colloidal particles can be described by (a) complete pore blocking model (CBM), (b) standard pore blocking model (SBM), (c) intermediate pore blocking model (IBM), and (d) cake filtration model (CFM). For the complete blocking, it is assumed that each

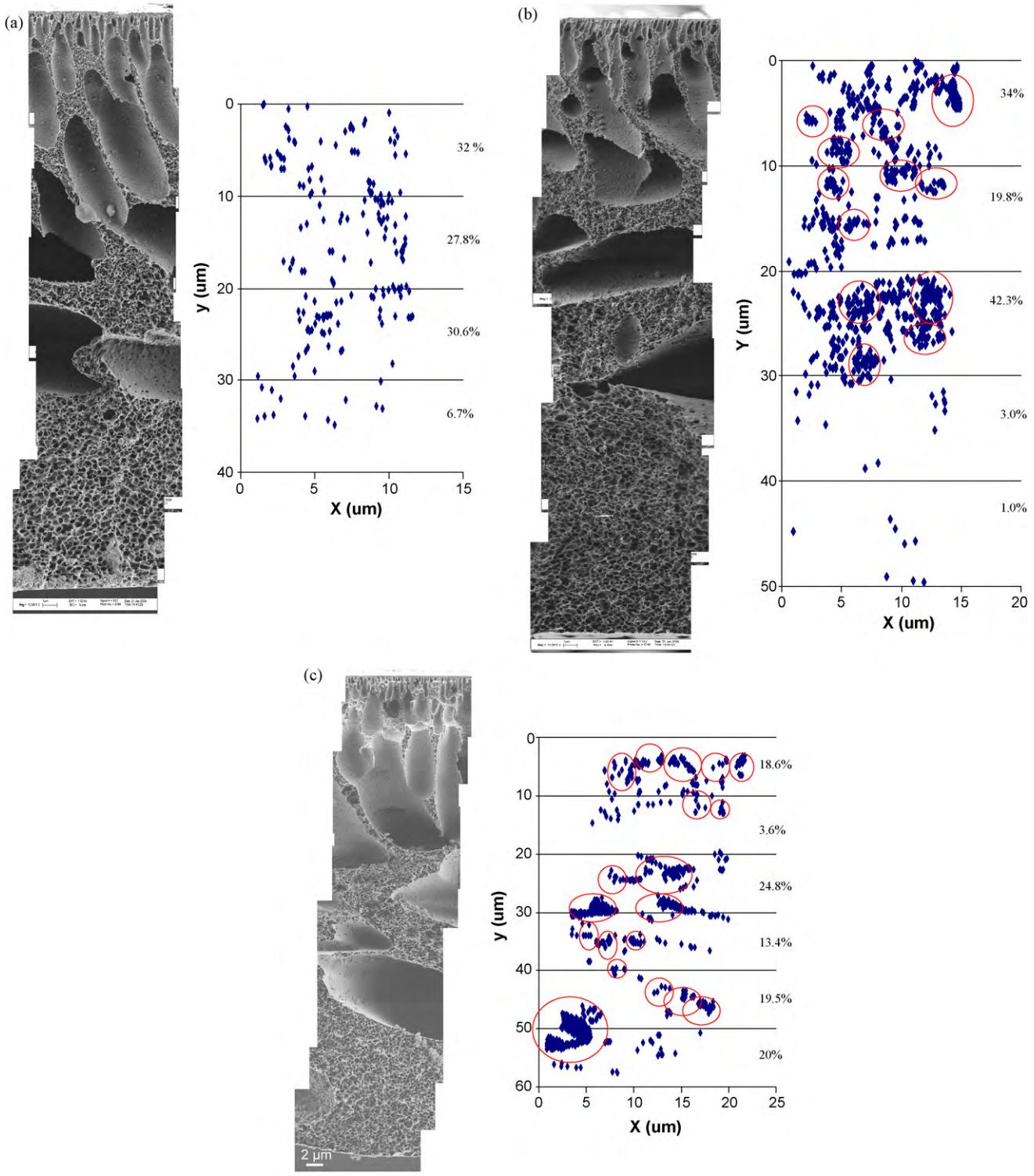

Fig. 1. (a) The Al_2O_3 distribution pattern in 0.03 Al_2O_3/PES (the scale bar represents 1 μm). (b) The Al_2O_3 distribution pattern in 0.05 Al_2O_3/PES (the scale bar represents 1 μm). (c) The Al_2O_3 distribution pattern in 0.1 Al_2O_3/PES membranes (the scale bar represents 2 μm).

particle reaching the membrane blocks a pore without superimposing over other particles. For the standard blocking, it is assumed that particles deposit within pores and the pore volume decreases proportionally to the volume of deposited particles. For the cake filtration, it is assumed that depositing particles do not block pores either because the membrane is dense and there are no pores to block, or because the pores are already covered by other particles and therefore are not available to block. For the intermediate blocking, it is assumed that some particles deposit on other particles (as in cake filtration) while other particles block membrane pores (as in complete blocking). The models also can be expressed as simple linear equations [29] relating the filtrate flow rate (Q), volume (V), and time (t) with the filtration constants for each model (K_b, K_i, K_s, K_c) and Q_o, the initial flow rate. In order to obtain the filtration constants K_b, K_i, K_s, K_c and Q_o the experimental data (Q and V or t) were plotted for each pore blocking model equations (Eq. (11)–(14)) [30].

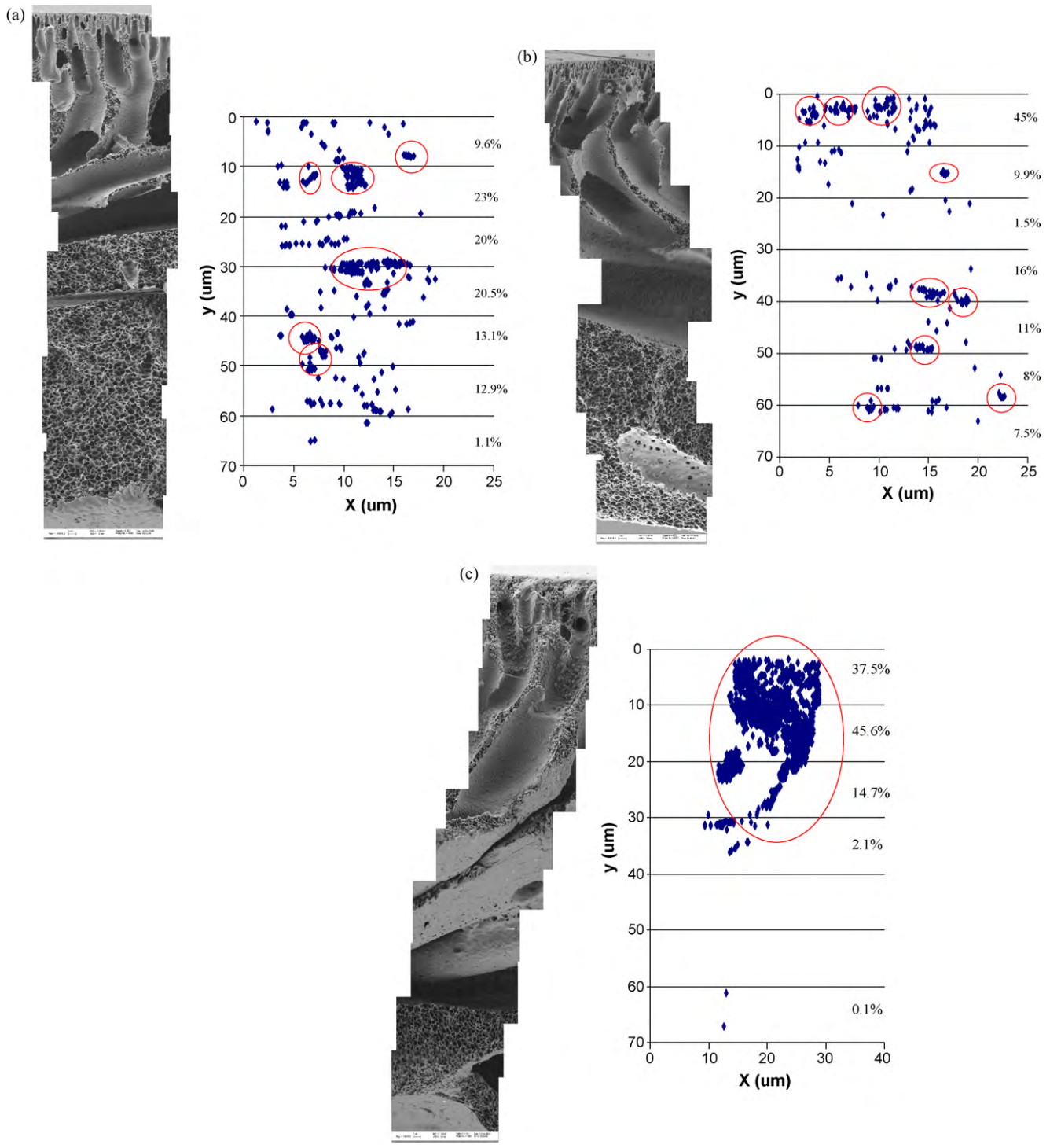

Fig. 2. (a) The ZrO_2 distribution pattern in 0.03 ZrO_2/PES membranes (the scale bar represents 1 μm). (b) The ZrO_2 distribution pattern in 0.05 ZrO_2/PES membranes (the scale bar represents 1 μm). (c) The ZrO_2 distribution pattern in 0.1 ZrO_2/PES membranes (the scale bar represents 1 μm).

Table 1
Membranes physical properties.

Physical properties	PES control	0.03 metal oxide/PES		0.05 metal oxide/PES		0.1 metal oxide/PES	
		Al_2O_3	ZrO_2	Al_2O_3	ZrO_2	Al_2O_3	ZrO_2
Membrane thickness (μm)	71.3 ± 1.4	34.7 ± 1.5	61.5 ± 6.9	49.3 ± 0.7	62.3 ± 5.3	56.5 ± 1.8	73.2 ± 2.5
Particle density (particles/μm^2)	0.0	0.51	0.368	1.21	0.277	0.98	0.551
Maximum TMP (bar)	1.724	1.034	2.758	1.034	2.758	1.724	3.1
MWCO (kDa)	600	600	600	200	600	200	600
Pore size (μm)	0.06–0.15	0.06–0.15	0.06–0.15	0.05–0.13	0.06–0.15	0.05–0.13	0.06–0.15

By smoothing each curve, a polynomial function can be obtained. The initial slope of the curve obtained at the value of V or t equals to zero allows the calculation of each filtration constant and the intercept is Q_o. The linear equations are:

$$Q = Q_o - k_b V \tag{11}$$

$$\frac{1}{Q} = K_i t + \frac{1}{Q_o} \tag{12}$$

$$\sqrt{Q} = \sqrt{Q_o} - \left(K_s \sqrt{Q_o}.\frac{V}{2}\right) \tag{13}$$

$$\frac{1}{Q} = \frac{1}{Q_o} + K_c V \tag{14}$$

where, Q is the volumetric flow rate; V is the filtrate volume; Q_o is the initial flow rate; K_b, K_i, K_s, K_c are the filtration constants for each model.

3. Results and discussion

3.1. Membrane morphology and structure

Fig. 1a–c shows the cross-section SEM pictures of Al_2O_3/PES membranes and the Al_2O_3 particles distribution pattern inside the membrane matrix with respect to membranes cross-sections with areas of 351, 651.9 and 877.3 μm^2 for 0.03, 0.05 and 0.1 Al_2O_3/PES membranes, respectively. Fig. 2a–c represents the cross-section SEM pictures of ZrO_2/PES membranes and ZrO_2 particles distributions with respect to membranes cross-sections with areas of 990.4, 944.8 and 1034 μm^2 for 0.03, 0.05 and 0.1 ZrO_2PES membranes, respectively. The X-axis and Y-axis represent the width and the length of the corresponding cross-section SEM pictures, respectively. The circles show the metal oxide particle aggregates. As apparent from the figures, the prepared membranes are skin-type membranes and show a structural change from a finger- to sponge-type structure. The percentage of sponge-like structure relative to the membrane structure was calculated by dividing the length of continuous network sponge (using SEM pictures) by the total membrane thickness (Y-axis). The finger structure is associated with high metal oxides percentage in the membrane matrix while the sponge-like structure was formed in the lower membrane layers (closest layer to the glass plate). It is well accepted that the most important features in immersion precipitation are the steep concentration and activity gradients of all components found in the polymer solution close to the polymer-precipitation medium interface [31]. Upon the immersion of polymer solution into a coagulation bath, the mass transfer which is normally expressed by the exchange rate of solvent/nonsolvent (NMP/water) at the interface between the polymer solution and the gelation medium, mainly determines the asymmetric structure of the membrane [31]. This exchange rate depends upon the nonsolvent tolerance of the polymer solution, the solvent viscosity and composition. Changing the composition of the casting solution or in the coagulation bath is a convenient method to obtain desired membrane structures. Adding solvents in the coagulation bath can delay the occurrence of liquid–liquid demixing in the casting solution and thus result in denser asymmetric membranes [32]. On the contrary, adding nonsolvent in the casting solution can increase the porosity of membranes. For example, adding two different nonsolvents in the polymer solution successfully elevated the porosity of asymmetric polysulfone membranes [33]. In addition, the membrane morphology is strongly affected by the amount of nonsolvent additives. Reuvers [34] reported that appropriate amount of nonsolvent additives enhanced the formation of macrovoids (finger-like pores) while too much nonsolvent suppressed their formation. Evaporating the casting solution before immersion in the coagulation bath is also a common treatment to improve the membrane structure [35]. It has been reported that evaporation is an efficient method to suppress the formation of macrovoids [36]. Generally lowering the precipitation rate results in a transition in morphology from a finger- to sponge-type structure [31]. Very high precipitation rates always lead to finger structures while slow precipitation rates lead to a sponge-like structures [31]. Since metal oxides have higher affinity for water than PES, the penetration velocity of water into the nascent membrane increases with the metal oxides content especially at the film surface and hence the concentration of precipitant (water) soon reaches a value resulting in phase separation. In the interior (near the glass plate), however, the precipitant concentration is still far below the limiting concentration for phase separation. Therefore, phase separation occurs initially at the surface of the film, where, due to the very steep gradient of the chemical potential of the polymer, there is a net movement of the polymer perpendicular to the surface which results in the formation of the membrane skin [31]. In addition, the metal oxides particles can change the activity coefficient of the polymer, the solvent or the precipitant. Zaslavsky and Miheeva [37] found that the inorganic additives can alter the polymer composition of the coexisting phases depending on the type and concentration of the salt which results in a shift in the phase boundaries during the phase inversion process and consequently the rate of precipitation which also leads to a change in the membrane structure [31]. The aforementioned authors reported an increased thermodynamic activity coefficients for the aqueous dextran-polyethyleneglycol phase with the addition of potassium chloride (KCl), potassium thiocyanate (KSCN) and potassium sulfate (K_2SO_4) at molar concentration of 0.1–1.0 moles/L. It is important to emphasize that the activity coefficient changes and the phase diagram for each system are unique and have to be determined experimentally, which was beyond the scope of this work.

3.2. Metal oxides particles distributions

As apparent from Figs. 1a–c and 2a–c, most of the metal oxides particles tended to locate between 0 and 30 μm of the membrane thickness with density significantly decreasing beyond that depth. For the 0.03 metal oxides/PES (w/w) membranes, the particles were fairly uniformly distributed with about 20–25% of the particles in each 10 μm layer througout membrane thickness. However, the 0.03 ZrO_2/PES membranes showed larger numbers of particle aggregates compared to the 0.03 Al_2O_3/PES membranes. For the 0.05 ZrO_2/PES membranes, 45% of the particles were located at 0–10 μm layer of the membrane versus 34% in 0.05 Al_2O_3/PES membranes. Both membranes showed numbers of particle aggregates. However, due to the high particle density of the 0.05 Al_2O_3/PES membranes, the number and the density of the particle aggregates were higher than those in 0.05 ZrO_2/PES. The phenomena of particles aggregation is further confirmed in the 0.1 metal oxides load. The 0.1 ZrO_2/PES showed the poorest distribution of the particles among all the tested membranes with more than 80% of the particles located in less than 200 μm^2 of the total membrane cross-section area of 1034 μm^2. However, the metal oxides particles were fairly distributed in the 0.1 Al_2O_3/PES membranes with considerable numbers of particles aggregates in different spots.

3.3. Membranes physical properties and performances

Table 1 shows the physical properties of the prepared membranes in terms of membrane thickness, particles density, maximum TMP sustained by the membranes, MWCO of the tested membranes using PEO and membrane pore size. As apparent from Table 1, the PES membrane thickness was slightly affected by the ZrO_2 particles additions; however, with the Al_2O_3 additions, the

Table 2
Statistical correlations factors (R) between membrane physical characteristics and membrane performances.

	Membrane thickness	Particle density	Maximum TMP	MWCO	Steady-state fouling rate	Steady-state permeability	R_t	R_c	R_f	DIW permeability
Membrane thickness	1									
Particle density	0.45	1								
Maximum TMP	**0.74**	−0.43	1							
MWCO	0.29	**−0.89**	0.51	1						
Steady-state fouling rate	0.43	−0.50	−0.19	0.12	1					
Steady-state permeability	**−0.75**	−0.5	−0.43	−0.31	−0.69	1				
R_t	0.64	−0.55	0.08	0.21	**0.94**	**−0.85**	1			
R_c	0.63	−0.59	−0.09	0.25	**0.94**	**−0.85**	**0.99**	1		
R_f	0.21	−0.23	−0.07	0.28	0.25	0.08	0.20	0.19	1	
DIW permeability	−0.07	−0.16	0.31	0.27	−0.45	0.54	−0.48	−0.46	0.23	1

The bold values highlight the good and strong correlations.

membranes thicknesses were reduced by 30–50% relative to the PES membrane. This observation coupled with the higher maximum TMP sustained by the ZrO_2/PES membranes than the control PES and Al_2O_3/PES membranes of the same metal oxides/PES ratios suggests that the PES casting solution viscosity and consequently its spreading on the glass plate during the phase inversion process may have been more affected by the addition of Al_2O_3 particles than the ZrO_2 particles. Table 2 shows the effects of the membrane physical characteristics on the membrane performances as reflected by different statistical correlation factors (R). The moderate direct statistical correlation ($R = 0.74$) observed between membrane thickness and maximum TMP further supports the previous discussion. The results showed that the MWCO of metal oxides/PES membranes and neat membranes are the same (600 kDa) with pore size ranging between 0.06 and 0.15 μm, except for the 0.05 and 0.1 Al_2O_3/PES membranes (MWCO of 200 kDa and membrane pore size of 0.05–0.13 μm). The moderate inverse statistical correlation ($R = 0.89$) observed between membrane metal oxides particle density and membrane MWCO may provide an explanation for the lower MWCO of 0.05 and 0.1 Al_2O_3/PES membranes as they exhibited the highest particle density among all tested membranes. It is also obvious from Table 2 that the membrane steady-state permeability and fouling rates are functions of membrane total and cake resistances. Since the membrane thickness, pore size, and MWCO in the neat and ZrO_2/PES membranes were comparable, it can be concluded that the presence of ZrO_2 particles has not exerted any negative effect on the PES membranes physical characteristics even at higher ZrO_2/PES ratios. However, it is deemed that the high loads of Al_2O_3 particles reduce PES membranes thicknesses, membranes MWCO, and pore sizes.

Table 3 represents the different membrane resistances, pseudo steady-state fouling rates, and steady-state permeabilities for tested membranes. It is apparent from Table 3 that all tested membranes have comparable membrane resistances (R_m) which indicates that the membrane resistance is mainly due to the type of membrane polymer and is relatively unaffected by the metal oxide particles. It is also obvious from Table 3 that the addition of the metal oxides particles has enhanced the PES performance by decreasing membranes cake and total resistances and increasing membrane permeability. In general, Al_2O_3/PES membranes showed lower pseudo steady-state fouling rates, higher pseudo steady-state permeabilities as well as lower cake and total resistances than the same load of ZrO_2/PES membranes. The higher pseudo steady-state permeability observed for the Al_2O_3/PES membranes relative to the ZrO_2/PES membranes at the same metal oxide/PES weight ratios (Table 3) may be attributed to the lower membrane thickness observed for the Al_2O_3/PES membranes relative to the ZrO_2/PES membranes at the same metal oxide/PES weight ratios (Table 1). This observation is further supported by the moderate inverse statistical correlation ($R = 0.75$), between membrane thickness and its pseudo steady-state permeability (Table 2). The higher fouling rate observed for the ZrO_2/PES membranes may be attributed to the larger pore size observed for theses membranes (Table 1). Fang and Shi [15] indicated that of the three membranes with sponge-like microstructure investigated, foulants had a much higher tendency to deposit inside the porous structure of the PES membrane with large pore openings (up to 18–20 μm) than inside the mixed cellulose ester (MCE) and polyvinylidene fluoride (PVDF) membranes with pore openings of 0.5–3 μm. The more foulant deposits resulted in the higher Rp.

3.4. DIW permeation

The DIW permeation profiles by different metal oxides/PES membranes are shown in Fig. 3. The values presented in this figure are the slopes of the straight lines generated by recording the DIW flux at different TMP (0.345, 0.6895 and 1.0342 bar) with R^2 values of 0.89–0.99. The Y-error bars represent the 95% confidence intervals. As apparent from Fig. 3, membrane DIW permeations increased with the increase of the metal oxides particles concentrations up to 0.05 metal oxides/PES and decreased thereafter. The DIW permeabilities for the ZrO_2/PES were about 1.8 times that of the PES, however, the permeabilities of Al_2O3/PES membranes were 1.2–1.4 times that of the neat membrane. It is worth noting that the permeability of 0.03 and 0.05 ZrO_2/PES membranes are 19% and 35% higher than those of the corresponding Al_2O_3/PES, which

Table 3
Membranes performances.

	PES control	0.03 metal oxide/PES		0.05 metal oxide/PES		0.1 metal oxide/PES	
		Al_2O_3	ZrO_2	Al_2O_3	ZrO_2	Al_2O_3	ZrO_2
Initial fouling rate (L/m^2 bar-h^2)	526.2	3301	3459	4387	3907	375	1172
Pseudo steady-state fouling rate (L/m^2 bar-h^2)	0.005	6.06E−07	2.72E−05	1.25E−11	2.37E−06	0.0011	3.05E−06
Pseudo steady-state permeability (y°) (L/m^2 bar-h)	20.4	202	121.3	252	194.9	94.5	56.6
R_m ($\times 10^7$ m^{-1})	0.34	0.39	0.33	0.32	0.32	0.61	0.46
R_f ($\times 10^7$ m^{-1})	1.13	0.79	0.82	1.16	0.83	0.33	0.96
R_c ($\times 10^7$ m^{-1})	6.2	0.61	1.8	0.32	0.91	2.3	2.13
R_t ($\times 10^7$ m^{-1})	7.6	1.79	3.0	1.8	2.2	3.7	3.56

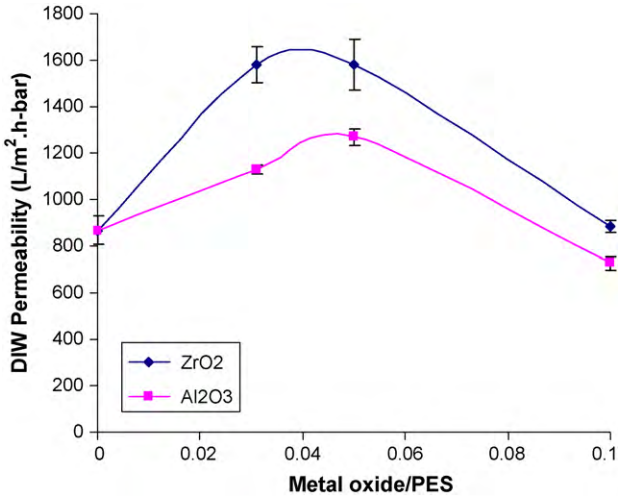

Fig. 3. DIW permeability for different metal oxides/PES membranes.

suggests that the pore sizes are much larger in case of ZrO_2/PES membranes. The lower DIW permeation of Al_2O_3/PES membranes may be attributed to the higher metal oxides particles density of the Al_2O_3/PES membranes relative to the ZrO_2/PES membranes at the same metal oxide/PES weight ratios (Table 1). This observation is further confirmed by the MWCO and pore size values determined for different membranes and the metal oxides particles density in the membrane matrix as discussed in the previous section (Section 3.3).

3.5. Correlation of membrane properties and performance with particles distributions

In order to ensure insightful understanding of the effect that metal oxides particles distribution may have on the membranes performances, statistical correlations between the metal oxide particles in each membrane depth (representing the *Y*-axis in Figs. 1a–c and 2a–c) with different membranes characteristics and performances parameters were studied. Table 4 presents correlation factors (R) between the metal oxides particles density at each membrane depth and membranes characteristics and performance parameters.

As apparent from Table 4, no statistical correlations have been observed between either the particles densities at the 0–10 or 10–20 μm depths and any membranes characteristics or performances parameters. This observation is consistent with the finding reported in Table 2, as no statistical correlations have been observed between metal oxides particle density and membrane characteristics or performance parameters except for membrane MWCO. Table 4 also shows the moderate inverse correlation (R = 0.72) between the metal oxides particles densities at a membrane depth of 20–30 μm and membrane MWCO. This inverse correlation is highly reflected in the 0.05 Al_2O_3/PES and 0.1 Al_2O_3/PES membranes with MWCO of 200 kDa, as these membranes have the highest particles densities of 2.59 and 1.37 particles/μm^2, respectively, at the 20–30 μm depth.

Surprisingly, strong inverse correlations with R of 0.84 and 0.95 were observed between the metal oxides particles densities at the membranes depths of 30–40 and 40–50 μm, respectively, and membrane fouling resistances (R_f). The perfect example for these correlations is the 0.1 Al_2O_3 with the lowest R_f value and highest particles densities of 0.74 and 1.08 particles/μm^2 at membrane depths of 30–40 and 40–50 μm, respectively. The decrease in R_f values with the increase in the particles density can be explained as follows: Eqs. (6) and (7) show that the R_m value depends on the value of J_{iw}, while the R_f value depends on the J_{fw}. When the membranes pores are already occupied with the metal oxides aggregates, the values of J_{fw} and J_{iw} were very close and consequently the R_f values become very small. It is worth noting that the membrane fouling is known to be impacted by extracellular polymeric substances (EPS) and soluble microbial products (SMP), which are a function of system operational conditions and nature of feed. In our previous work [38], a comparison between the chemical characteristics of EPS and SMP and their effect on membrane fouling in two MBR applications, comprising a conventional MBR (C-MBR) treating synthetic wastewater (identical in composition to the one used here) and biological nutrient removal MBR (BNR-MBR) treating real wastewater, was conducted. The aforementioned study concluded that in the BNR-MBR system, the membrane fouling and consequently membrane total resistance has decreased due to increased hydrophobicity of EPS resulting in higher floc agglomeration and greater porosity of flocs. However, the membrane fouling and the membrane pore plugging (i.e., R_f) increased with increasing SMP concentration and hydrophobicity which were higher in the C-MBR system. Since the membrane fouling resistance in the current study was measured using sludge cultivated in a C-MBR treating synthetic wastewater, it is expected that the membrane fouling resistance will be enhanced during filtration of sludges cultivated by real wastewater.

Although no statistical correlations were observed between DIW permeability and particles densities at each membrane depth, the higher DIW permeability observed for ZrO_2/PES membranes relative to Al_2O_3/PES membranes may be attributed to their higher percentage of the finger structure (41%, 62% and 79% for 0.03, 0.05 and 0.1 ZrO_2/PES membranes, respectively) compared to the corresponding loads of Al_2O_3/PES membranes (40%, 52% and 65%, respectively). It is well accepted that the finger structure is more permeable than the sponge structure [31]. Therefore, as the membrane morphology exhibits a high percentage of finger structure, the DIW permeability is expected to increase. However, the increase in the DIW permeability as shown in Fig. 3 is not linear, as

Table 4
Statistical correlations (R) between metal oxides nanoparticles densities at different membrane thickness and membranes characteristics and performances parameters.

	Membranes depth				
	0–10 μm	10–20 μm	20–30 μm	30–40 μm	40–50 μm
Membrane thickness	0.28	0.39	−0.16	0.01	−0.40
Maximum TMP	0.47	0.33	−0.25	0.25	−0.16
MWCO	0.16	−0.11	**−0.72**	−0.46	−0.55
Steady-state fouling rate	−0.32	−0.40	−0.41	−0.35	−0.12
Steady-state permeability	−0.26	−0.07	0.30	−0.06	−0.057
R_t	−0.09	−0.22	−0.38	−0.24	−0.12
R_c	−0.11	−0.26	−0.42	−0.24	−0.12
R_f	0.23	0.18	0.10	**−0.84**	**−0.95**
DIW permeability	−0.25	−0.27	−0.23	0.00	−0.29

The bold values highlight the good and strong correlations.

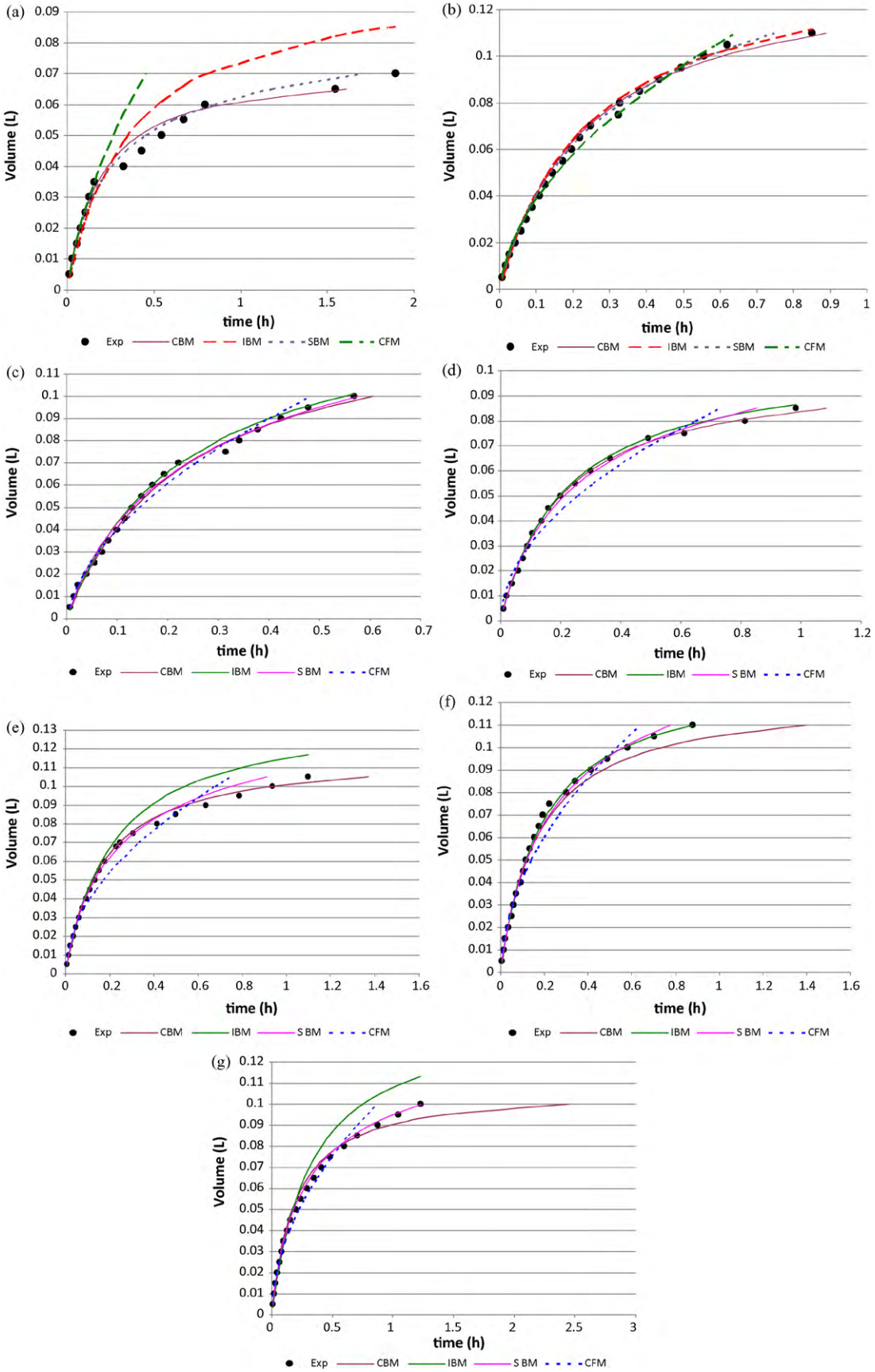

Fig. 4. *V–t* curves estimated from the constant pressure filtration models and experimental data for a sludge filtration. (a) PES membrane, (b) 0.03 Al_2O_3/PES membranes, (c) 0.05 Al_2O_3/PES, (d) 0.1 Al_2O_3/PES membranes, (e) 0.03 ZrO_2/PES, (f) 0.05 ZrO_2/PES membranes and (g) 0.1 ZrO_2/PES.

the highest load of the metal oxide plugged membranes pores and led to a decrease in DIW permeability (Fig. 3).

It is worth noting that the DIW permeability trend is consistent with the membranes steady-state permeability observed for all tested membranes. For example, the DIW permeability for 0.05 Al_2O_3/PES membranes is 11% and 42% higher than that of 0.03 Al_2O_3/PES membranes and 0.1 Al_2O_3/PES membranes, respectively. Similarly, the pseudo steady-state permeability for 0.05 Al_2O_3/PES membranes is 20% and 38% higher than that of 0.03 Al_2O_3/PES membranes and 0.1 Al_2O_3/PES membranes, respectively.

3.6. Fouling mechanism

The filtration constants and initial flow rates (Q_0) for different constant pressure filtration models were obtained by fitting the experimental results with the simple linear equations (Eqs. (11)–(14)). Using the slopes and intercepts, filtration constants and initial flow rate were determined and then substituted into the equations (Eqs. (11)–(14)) to estimate the values of V and t for each model. A comparison between the theoretical and the experimental V and t values for the neat and metal oxides/PES membranes are presented in Fig. 4a–g. As apparent from the figures, all tested membranes, except the neat PES and 0.1 Al_2O_3/PES membranes only, showed initial fouling due to the four aforementioned models (up to 0.1 h filtration time) which may provide an explanation for the high initial fouling rate observed for the other metal oxides/PES membranes. For the neat PES and 0.1 Al_2O_3/PES membranes, which showed low initial fouling rates of 526.2 and 375 L/m^2 bar-h^2, respectively, the CFM model deviated from the experimental results which suggests that the formation of cake layer at the initial stage of filtration is the main reason for the high initial fouling rate observed for the other membranes (Table 3). With time, the main fouling mechanism for all tested membranes (Fig. 4a–g) appeared to be the standard pore blocking except for the 0.1 Al_2O_3/PES and 0.03 ZrO_2/PES membranes which showed a complete pore plugging mechanism. Fan and Shi [15] concluded that membranes with sponge-like structure are more vulnerable to pore fouling due to their porous network. Fig. 2a shows that around 59% of the 0.03 ZrO_2/PES structure is in a sponge-type (the highest sponge-like structure of all tested membranes) which may explain the CBM mechanism observed for this membrane. For the 0.1 Al_2O_3/PES (Fig. 1c), the CBM fouling mechanism pertains despite the fact that only 35% of the membrane structure was a sponge-type, can be explained based on the relation between precipitation rate and pore size detailed further. Porter [31] concluded that if a sponge-like structure is obtained, the pore diameters are inversely proportional to the rate of precipitation. Higher precipitation rates (within the sponge-like structure) lead to finer pore structures. Since 0.1 Al_2O_3/PES showed the highest metal oxide particles density of 1.08 and 1.108 particles/μm^2 at 40–50 and 50–60 μm of membrane depth, respectively (i.e., at the sponge-like structure), the precipitation rate within the sponge-like structure was relatively high and lead to finer pore structures that can be easily blocked completely during sludge filtration. It is important to emphasize few aspects of filtration that probably led to these complicated observations. First, the models are based on single pore size in contrast to the range of pore sizes (Table 1) and a change in the membrane morphology from finger to sponge-type structure (Figs. 1a–c and 2a–c). Secondly, the models are based on uniform spherical particles being the foulant [39] in contrast to the wide range of the particles sizes distributions found usually in the sludge [38] probably resulting in a combination of different fouling mechanisms. Thus, no significant correlations between the metal oxides distribution patterns and the fouling mechanism for the tested membranes were observed.

4. Conclusions

This research aimed at shedding more light on the role of metal oxide particles distribution pattern inside the membrane matrix on in the metal oxides/PES membranes characteristics and performances during sludge filtrations. The major findings from this study are:

1. The prepared metal oxides/PES membranes are skin-type membranes and show a structural change from a finger- to sponge-type structure depending on metal oxide distribution.
2. Allthough, the PES membrane thickness was slightly affected by the ZrO_2 particles additions; the Al_2O_3 additions significantly reduced the membranes thicknesses by 30–50%.
3. No statistical correlations have been observed between either the particles densities at the 0–10 or 10–20 μm depths and any membranes physical characteristics or performances parameters. However, inverse moderate correlation ($R = 0.72$) between the metal oxides particles densities at membrane depth of 20–30 μm and membrane MWCO was observed.
4. Strong inverse correlations with R of 0.84 and 0.95 were observed between the metal oxides particles densities at the membranes depths of 30–40 and 40–50 μm, respectively, and membrane fouling resistances (R_f).
5. According to the constant pressure models, the experimental results for sludge filtration using all tested membranes were in good agreement with SBM model.

Acknowledgement

The authors would like to thank Solvay Advanced Polymers, Alpharetta, GA, USA for supplying the PES polymer

References

[1] A.D. Marshall, P.A. Munro, G. Tragardh, The effect of protein fouling in microfiltration and ultrafiltration on permeate flux, protein retention and selectivity: a literature review, Desalination 91 (1993) 65–108.
[2] A.G. Fane, C.J.D. Fell, A review of fouling and fouling control in ultrafiltration, Desalination 62 (1987) 117–136.
[3] E. Matthiasson, The role of macromolecular adsorption in fouling of ultrafiltration membranes, J. Membr. Sci. 16 (1983) 23–36.
[4] J.L. Nilsson, Protein fouling of uf membranes: causes and consequences, J. Membr. Sci. 52 (1990) 121–142.
[5] S. Metsamuuronen, J. Howell, M. Nystrom, Critical flux in ultrafiltration of myoglobin and baker's yeast, J. Membr. Sci. 196 (2002) 13–25.
[6] R. Molinari, M. Mungari, E. Drioli, A.D. Paola, V. Loddo, L. Palmisano, M. Schiavello, Study on a photocatalytic membrane reactor for water purification, Catal. Today 55 (2000) 71–78.
[7] R. Molinari, C. Grande, E. Drioli, L. Palmisano, M. Schiavello, Photocatalytic membrane reactors for degradation of organic pollutants in water, Catal. Today 67 (2001) 273–279.
[8] R. Molinari, L. Palmisano, E. Drioli, M. Schiavello, Studies on various reactors configurations for coupling photocatalysis and membrane process in water purification, J. Membr. Sci. 206 (2002) 399–415.
[9] S.Y. Kwak, S.H. Kim, S.S. Kim, Hybrid organic/inorganic reverse osmosis (RO) membrane for bactericidal anti-fouling. 1. Preparation and characterization of TiO_2 nanoparticle self-assembled aromatic polyamide thin film composite (TFC) membrane, Environ. Sci. Technol. 35 (2001) 2388–2394.
[10] S.H. Kim, S.Y. Kwak, B.H. Sohn, T.H. Park, Design of TiO_2 nanoparticle self-assembled aromatic polyamide thin-film-composite (TFC) membrane as an approach to solve biofouling problem, J. Membr. Sci. 211 (2003) 157–165.
[11] T.H. Bae, T.-M. Tak, Effect of TiO_2 nanoparticles on fouling mitigation of ultrafiltration membranes for activated sludge filtration, J. Membr. Sci. 249 (2005) 1–8.
[12] N. Maximous, G. Nakhla, W. Wan, K. Wong, Preparation, characterization and performance of Al_2O_3/PES membrane for wastewater filtration, J. Membr. Sci. 341 (2009) 67–75.
[13] N. Maximous, G. Nakhla, W. Wan, K. Wong, Optimization of Al_2O_3/PES membrane for water filtration, J. Sep. Purif. Technol. 73 (2010) 294–301.
[14] N. Maximous, G. Nakhla, W. Wan, K. Wong, Performance of a novel ZrO_2/PES membrane for wastewater filtration, J. Membr. Sci. 352 (2010) 222–230.
[15] H.H.P. Fang, X. Shi, Pore fouling of microfiltration membranes by activated sludge, J. Membr. Sci. 264 (2005) 161–166.

[16] Y. He, P. Xu, C. Li, B. Zhang, High-concentration food wastewater treatment by an anaerobic membrane bioreactor, Water Res. 39 (2005) 4110–4118.
[17] P. Le-Clech, B. Jefferson, S.J. Judd, Impact of aeration, solids concentration and membrane characteristics on the hydraulic performance of a membrane bioreactor, J. Membr. Sci. 218 (2003) 117–129.
[18] I.S. Chang, M. Gander, B. Jefferson, S.J. Judd, Low-cost membranes for use in a submerged MBR, Proc. Saf. Environ. Prot. 79 (2001) 183–188.
[19] S.S. Madaeni, A.G. Fane, D.E. Wiley, Factors influencing critical flux in membrane filtration of activated sludge, J. Chem. Technol. Biotechnol. 74 (1999) 539–543.
[20] I.-S. Chang, K.-H. Choo, C.-H. Lee, U.-H. Pek, U.-C. Koh, S.-W. Kim, J.-H. Koh, Application of ceramic membrane as a pretreatment in anaerobic digestion of alcohol-distillery wastes, J. Membr. Sci. 90 (1994) 131–139.
[21] I.S. Chang, P. Le-Clech, B. Jefferson, S. Judd, Membrane fouling in membrane bioreactors for wastewater treatment, J. Environ. Eng. ASCE 128 (2002) 1018–1029.
[22] M. Mulder, Basic Principles of Membrane Technology, Kluwer Academic Publishers, 1996, p. 383.
[23] K.J. Kim, A.G. Fane, R. Ben Aim, M.G. Liu, G. Joansson, I.C. Tessaro, A.P. Broek, D. Bargeman, A comparative study of techniques used for porous membrane characterization: pore characterization, J. Membr. Sci. 87 (1994) 35–46.
[24] H. Lee, R.M. Venable, A.D. MacKerell Jr., R.W. Pastor, Molecular dynamics studies of polyethylene oxide and polyethylene glycol: hydrodynamic radius and shape anisotropy, J. Biophys. 95 (2008) 1590–1599.
[25] T.K. Rostovtseva, E.M. Nestorovich, S.M. Bezrukov, Partitioning of differently sized poly(ethylene glycol)s into OmpF porin, J. Biophys. 82 (2002) 160–169.
[26] K. Devanand, J.C. Selser, Asymptotic-behavior and long-range interactions in aqueous-solutions of poly (ethylene oxide), Macromolecules 24 (1991) 5943–5947.
[27] C. Tanford, Physical Chemistry of Macromolecules, John Wiley & Sons, New York, 1961.
[28] J. Hermia, Constant pressure blocking filtration law application to power-law non-newtonion fluid, Trans. Inst. Chem. Eng. 60 (1982) 183–187.
[29] K. Matsumoto, S. Kutsuyama, H. Ohya, Separation of yeast by crossflow filtration with backwashing, J. Ferment. Technol. 65 (1987) 77–83.
[30] R. Jiraratananon, D. Ulttapap, P. Sampranpiboon, Cross flow microfiltration of a colloidal suspension with the presence of macromolecules, J. Membr. Sci. 140 (1998) 57–66.
[31] M.C. Porter, Handbook of Industrial Membrane Technology, Noyes Publications, Park Ridge, NJ, USA, 1990.
[32] C.A. Smolders, A.J. Reuvers, R.M. Boom, I.M. Wienk, Microstructures in phase-inversion membranes. Part 1. Formation of macrovoids, J. Membr. Sci. 73 (1992) 259–275.
[33] S.C. Pesek, W.J. Koros, Aqueous quenched asymmetric polysulfone membranes prepared by dry/wet phase separation, J. Membr. Sci. 81 (1993) 71–88.
[34] A.J. Reuvers, Membrane formation: diffusion induced demixing processes in ternary systems, Ph.D. Thesis, Twente University of Technology, The Netherlands, 1987.
[35] B. Kunst, S. Sourirajan, Evaporation rate and equilibrium phase separation data in relation to casting conditions and performance of porous cellulose acetate reverse osmosis membranes, J. Appl. Polym. Sci. 14 (1970) 1983–1996.
[36] F.G. Paulsen, S.S. Shojaie, W.B. Krantz, Effect of evaporation step on macrovoid formation in wet-cast polymeric membranes, J. Membr. Sci. 91 (1994) 265–282.
[37] B.Y. Zaslavsky, L.M. Miheeva, Influence of inorganic electrolytes on partitioning of non-ionic solutes in an aqueous dextran-poly(ethyleneglycol) biphasic system, J. Chromatogr. 392 (1987) 95–100.
[38] N. Maximous, S. Arabi, M. Kim, G. Nakhla, Comparison of biofoulants in BNR-MBR and conventional MBR (C-MBR) systems WEFTEC conference, October 18–22, McCormick Place Chicago, IL, 2008.
[39] F. Wang, V.V. Tarabara, Pore blocking mechanism during early stages of membrane fouling by colloids, J. Colloid Interface Sci. 328 (2008) 464–469.